J. Fluid Mech. (1988), *vol.* 192, *pp.* 1–16
Printed in Great Britain

Shocks and singularities in the pressure field of a supersonically rotating propeller

By C. J. CHAPMAN
Institute of Sound and Vibration Research, University of Southampton, Southampton SO9 5NH, UK

(Received 1 July 1987)

When linear acoustic theory is applied to the thickness noise problem of a supersonic propeller, it can give rise to a surface on which the pressure is discontinuous or singular. A method is described for obtaining the equation of this surface (when it exists), and the pressure field nearby; jumps, logarithms and inverse square roots occur, and their coefficients may be calculated exactly. The special case of a blade with a straight radial edge gives a cusped cone, whose sheets, each with a different type of discontinuity or singularity in pressure, are separated by lines of cusps; the coefficients in formulae for the pressure near the surface tend to infinity as a cusp line is approached, in proportion to the inverse quarter power of distance from the line. These results determine regions of space where nonlinear effects are important, and they suggest a strong analogy with sonic boom.

1. Introduction

Several investigators of propeller acoustics have noted that linear theory can give singularities in the pressure field. Hawkings & Lowson (1974) found a logarithm, and Tam (1983) an inverse square root, for sharp and blunt propeller edges, respectively; and singularities also occur implicitly in results of numerical studies, where they take the form of spikes truncated down to finite size (e.g. Farassat 1975; Hanson 1976; Blackburn 1984). The logarithm and inverse square root were found through the non-convergence, in certain regions of space, of a Fourier series representing the pressure in the far field; the whole surface of infinite pressure (on linear theory) was not revealed.

Now singularities in solutions of the scalar wave equation have been encountered in acoustic problems unrelated to propellers, and a particularly effective time-domain method for their analysis was given by Friedlander (1958, pp. 67–70), where a logarithm was shown to arise from the focusing of an acoustic shock. This paper applies Friedlander's method to the thickness noise problem of a supersonic propeller, to determine the surface on which the pressure is discontinuous or singular, and to obtain general formulae for the behaviour of the pressure near that surface. The special case of a propeller with a straight radial leading or trailing edge, and no axial motion, is discussed in detail, as an illustration of the theory. We shall use the term 'shock' to mean an acoustic shock, i.e. a finite discontinuity in the pressure.

A fact to emerge is the similarity between propeller theory and 'boom' analysis; especially relevant is the problem of an accelerating or manoeuvring aeroplane, or one flying through a non-uniform atmosphere (Lilley *et al.* 1953; Rao 1956; Guiraud 1965; Warren 1968; Hayes 1971; Wanner *et al.* 1972). Further references may be found in the proceedings of the three NASA conferences on sonic boom (Seebass

1967; Schwartz 1968, 1971). The difficult problem of how nonlinear effects eliminate the singularities of linear theory was begun in some of these papers, and continued in, for example, Gill & Seebass (1975), Cramer & Seebass (1978) and Obermeier (1983).

2. The integral for thickness noise

In its undisturbed state, the air is taken to be motionless and of uniform pressure, density, and sound speed, denoted p_0, ρ_0 and c, respectively. We shall take the propeller blades to be sufficiently thin that the usual assumptions of thin aerofoil theory apply. Viscous effects will be neglected, so that a velocity potential ϕ may be introduced, in terms of which the velocity is $\boldsymbol{u} = \nabla\phi$ and the perturbation pressure is $p = -\rho_0 \partial\phi/\partial t$. Only pressure and velocity fields rigidly attached to the propeller and rotating with it are of interest; to describe them we introduce cylindrical polar coordinates (r, θ', z), with respect to which the propeller is rotating about the z-axis at angular velocity $\Omega \boldsymbol{e}_z$, where Ω is constant and $\boldsymbol{e}_z$ denotes a unit coordinate vector. We take the translational velocity to be zero, and the propeller to lie across the plane $z = 0$. Then the relevant solutions are functions of (r, θ, z) only, where $\theta = \theta' - \Omega t$; the operator $\partial/\partial t$ may be replaced by $-\Omega\partial/\partial\theta$. Since we are considering thickness noise, the propeller is assumed to have the symmetric profile $z = \pm f(r, \theta)$, with f defined for all r, θ and given the value zero off the planform of the blades. Thus $\partial\phi/\partial z = \pm\Omega g$ on $z = \pm 0$, where $g \equiv \partial f/\partial\theta$. Typical f and g are drawn in figure 1.

The solution of the wave equation for ϕ, subject to the above boundary condition and suitable behaviour at infinity, is well known (Farassat 1975; Hanson 1976) from the Ffowcs Williams–Hawkings equation, and will be quoted. We require the integral

$$I(r, \theta, z) = \int_0^{2\pi} \int_0^{\infty} \frac{g(r_1, \Theta)}{R} r_1 \, \mathrm{d}r_1 \, \mathrm{d}\theta_1, \tag{1}$$

where

$$R = (r^2 + r_1^2 - 2rr_1 \cos\theta_1 + z^2)^{\frac{1}{2}}, \tag{2}$$

and

$$\Theta = \theta - \theta_1 + \Omega R/c; \tag{3}$$

then

$$\phi = \frac{\Omega I}{2\pi}, \quad p = \frac{\rho_0 \Omega^2}{2\pi} \frac{\partial I}{\partial\theta}. \tag{4}$$

Now $g(r, \theta)$ has lines of discontinuity or singularity at positions corresponding to the leading and trailing edges of the propeller blades, as indicated in figure 1; and $g(r_1, \Theta)$, regarded as a function of r_1, θ_1 at fixed r, θ, z, behaves similarly. Thus although $I(r, \theta, z)$ is continuous, the derivative $\partial I/\partial\theta$ appearing in p is not, and a question arises: how are the discontinuities and singularities in p related to those in g? We answer this question below.

3. Shocks and singularities

3.1. *Effect of leading and trailing edges*

We shall usually take r, z as fixed and regard θ as a variable; arguments r, z will often be omitted from the notation. Accordingly, the integral (1) will be written $I(\theta)$, so that $p \propto I'(\theta)$. If the position of an edge is given by an equation $h(r, \theta) = 0$, then the integrand in (1) is discontinuous or singular on a surface in (θ, r_1, θ_1)-space defined by

$$h(r_1, \theta - \theta_1 + \Omega R/c) = 0. \tag{5}$$

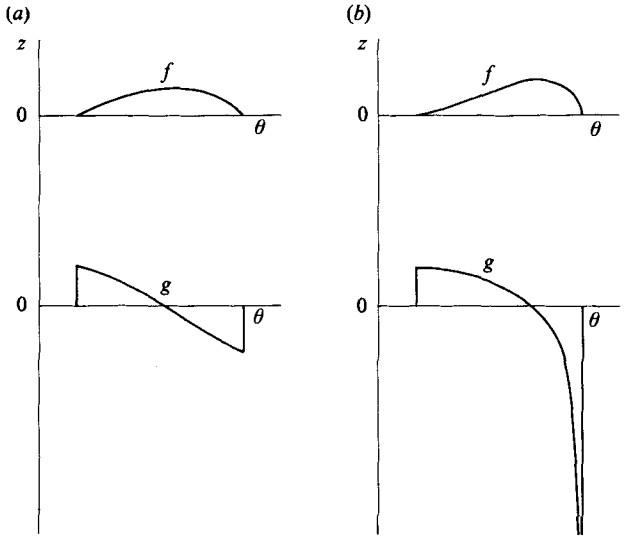

FIGURE 1. Graphs of $f(r,\theta)$ and $g(r,\theta)$ with r fixed. (*a*) Sharp leading and trailing edges; (*b*) blunt leading edge, sharp trailing edge.

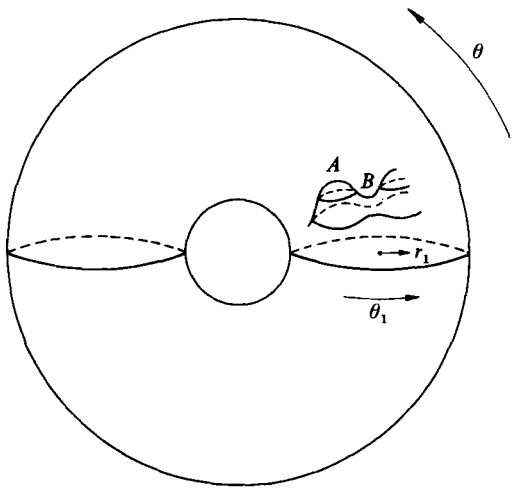

FIGURE 2. A typical part of the surface DS within a solid torus. The function $\theta = s(r_1,\theta_1)$ is stationary at A (maximum) and B (saddle). Contours of constant θ are shown.

In principle, this equation may be solved for θ and the surface written $\theta = s(r_1,\theta_1)$; it will be called the *dividing surface*, abbreviated DS. Since θ and θ_1 are angular variables, i.e. functions of them have period 2π, we may regard DS as lying in a solid torus, as shown schematically in figure 2. For simplicity, subsequent diagrams will be drawn as if θ, r_1, θ_1 were rectangular Cartesian coordinates, with θ pointing upwards; thus the integral (1) corresponds to taking a horizontal section at fixed θ, which will intersect DS in one or more curves.

Let us consider the behaviour of g near DS by following a vertical line of increasing θ at fixed r_1, θ_1. Since R does not depend on θ, the function $g(r_1, \Theta)$ on the vertical line is the function g shown in figure 1, but with a shift depending on the values of r_1 and θ_1. Therefore if the edge defined by $h(r,\theta)$ is a sharp leading edge, the passage

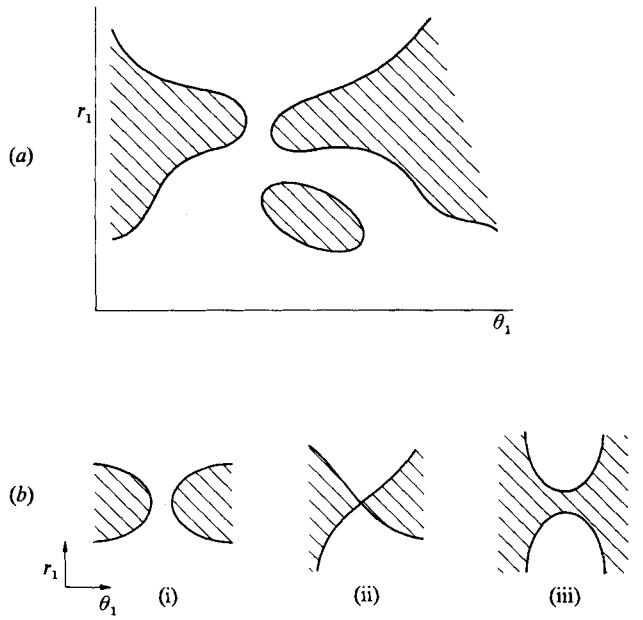

FIGURE 3. (*a*) At a fixed section θ, regions of non-zero $g(r_1, \Theta)$ are shaded; boundaries mark intersections of DS with the section. (*b*) Regions joining up, as θ varies.

upwards through DS marks a discontinuity in g from a negative value to zero; indeed, g is zero in a volume above the surface. For a blunt leading edge, $g \to -\infty$ in proportion to an inverse square root as DS is approached from below, and then it becomes zero above the surface. Trailing edges lead to similar results, but with g zero below DS and non-zero above.

Figure 3(*a*) shows a section at constant θ and the corresponding division of the (r_1, θ_1)-plane into different regions, bounded by curves in which DS intersects the section. These regions constitute the propeller blades looked at in retarded time, and determine the domain of integration for (1), i.e. the region of non-zero integrand; the topological character changes as θ passes through values of stationary points of DS, since at a maximum or minimum an 'island' is born or dies, and at a saddle point the regions join up or separate, as in figure 3(*b*). At these values, $I'(\theta)$ is discontinuous or singular; but elsewhere $I'(\theta)$ is smooth, since the dividing curves move smoothly as a function of θ.

Now r and z have been fixed in the above discussion. Thus for given r, z we obtain a set of values of θ at which the function $\theta = s(r_1, \theta_1)$, defined implicitly by (5), is stationary; the resulting points (r, θ, z) form a surface SS in (physical) space around the propeller, precisely the surface on which shocks and singularities will be found. For each point on the surface, a local analysis of DS in (θ, r_1, θ_1)-space, coupled with the behaviour of g in its vicinity, will determine the nature and strength of the shock or singularity.

We may also obtain SS as an envelope of a two-parameter family of spheres. Equivalently, one may start with the envelope of the one-parameter family of spheres produced by a rotating point source, as calculated by Lowson & Jupe (1974); if each supersonic point on the propeller edge were regarded as producing such a surface, then the envelope would give SS.

3.2. *General formulae*

The behaviour of p near a critical value of θ will now be described. Four cases occur, from combinations of either an extremum or saddle point on DS, and either a sharp or blunt propeller edge; although a chord section with a blunt edge violates the thin aerofoil assumption, existing computer codes based on linear theory accept such a section as input, and the results below are therefore of some interest. Leading terms of two Taylor expansions about each critical point of DS are required, one for the integrand of (1), the other for $s(r_1, \theta_1)$. The resulting integrals can be evaluated exactly, and the degree of approximation in p calculated. Details are given in the Appendix, from which the formulae of this section may easily be verified.

3.2.1. *Sharp edge*; *extremum*

We consider a sharp leading edge, and for definiteness take θ_c to be a local maximum of DS, since this case arises in an example later (a subscript c will always indicate evaluation at a critical point). The Hessian

$$H = \frac{\partial^2 s}{\partial r_1^2}\frac{\partial^2 s}{\partial \theta_1^2} - \left(\frac{\partial^2 s}{\partial r_1 \partial \theta_1}\right)^2 \tag{6}$$

will be needed at the point determined by $\theta_c = s(r_{1c}, \theta_{1c})$; by assumption, $H > 0$. We put

$$\Delta p = p(r, \theta_c^+, z) - p(r, \theta_c^-, z), \tag{7}$$

and let g^- denote the limiting value of $g(r_1, \Theta)$ as DS is approached from vertically below the critical point, so that Δp and g^- are functions of position on the surface SS. Then by (A 5),

$$\Delta p = \rho_0 \Omega^2 \left(\frac{r_1 g^-}{R H^{\frac{1}{2}}}\right)_c. \tag{8}$$

For an angled trailing edge, we let g^+ be the limit of $g(r_1, \Theta)$ as DS is approached from above, and in (8) replace g^- by $-g^+$ to obtain the corresponding Δp. Note that g^+ refers to the position just ahead of the trailing edge, g^- to that just behind the leading edge.

3.2.2. *Sharp edge*; *saddle*

If θ_c is a critical value corresponding to a saddle point on DS, then $H < 0$, and the singular part p_s of the pressure near SS, in the case of a sharp leading edge, is

$$p_s = -\frac{\rho_0 \Omega^2}{\pi}\left(\frac{r_1 g^-}{R(-H)^{\frac{1}{2}}}\right)_c \ln\left(\frac{1}{|\theta - \theta_c|}\right), \tag{9}$$

by (A 6). A trailing edge requires $-g^+$ instead of g^-.

3.2.3. *Blunt edge*; *extremum*

It will be assumed that f in figure 1 (*b*) behaves like a square root at a blunt edge $h(r, \theta) = 0$, which we rewrite as $\theta = h_1(r)$, so that g nearby takes the form

$$g(r, \theta) = \frac{g_1(r, \theta)}{|\theta - h_1(r)|^{\frac{1}{2}}}. \tag{10}$$

On the side occupied by the blade, g_1 is bounded, and on the other side it is zero. From (A 7), a local maximum on DS gives

$$p_s = \begin{cases} -\rho_0 \Omega^2 \left(\dfrac{r_1 g_1^-}{RH^{\frac{1}{2}}}\right)_c \dfrac{1}{(\theta_c - \theta)^{\frac{1}{2}}} & (\theta < \theta_c) \quad \text{(leading edge)}, \\ -\rho_0 \Omega^2 \left(\dfrac{r_1 g_1^+}{RH^{\frac{1}{2}}}\right)_c \dfrac{1}{(\theta - \theta_c)^{\frac{1}{2}}} & (\theta > \theta_c) \quad \text{(trailing edge)}; \end{cases} \tag{11}$$

these are one-sided singularities, since the pressure tends to a finite limit as $\theta \to \theta_c$ from the opposite direction.

3.2.4. *Blunt edge; saddle*

By (A 8), this case gives one-sided singularities

$$p_s = \begin{cases} -\rho_0 \Omega^2 \left(\dfrac{r_1 g_1^-}{R(-H)^{\frac{1}{2}}}\right)_c \dfrac{1}{(\theta - \theta_c)^{\frac{1}{2}}} & (\theta > \theta_c) \quad \text{(leading edge)}, \\ \rho_0 \Omega^2 \left(\dfrac{r_1 g_1^+}{R(-H)^{\frac{1}{2}}}\right)_c \dfrac{1}{(\theta_c - \theta)^{\frac{1}{2}}} & (\theta < \theta_c) \quad \text{(trailing edge)}. \end{cases} \tag{12}$$

In (9)–(12), note that g^+, g_1^+ are positive, and g^-, g_1^- negative.

4. Application to a radial edge

4.1. *Particular form of the equations*

An infinitely long straight radial edge lying on $\theta = 0$ gives $h(r, \theta) \equiv \theta$; thus on scaling lengths by the sonic radius c/Ω, so that the propeller has sonic velocity at unit radius, (5) becomes

$$\theta = \theta_1 - R. \tag{13}$$

At fixed r, z this defines the equation $\theta = s(r_1, \theta_1)$ of DS. Stationary points are obtained from

$$\frac{\partial \theta}{\partial r_1} = -\frac{r_1 - r\cos\theta_1}{R} = 0, \tag{14}$$

$$\frac{\partial \theta}{\partial \theta_1} = 1 - \frac{r r_1 \sin\theta_1}{R} = 0, \tag{15}$$

i.e.

$$R = \tfrac{1}{2} r^2 \sin 2\theta_1, \tag{16}$$

$$R^2 = \tfrac{1}{2} r^2 (1 - \cos 2\theta_1) + z^2; \tag{17}$$

hence

$$(r^2 \cos 2\theta_1 - 1)^2 = (r^2 - 1)^2 - 4z^2, \tag{18}$$

and

$$\theta = \tfrac{1}{2} \cos^{-1}\left[\frac{1 \pm \{(r^2-1)^2 - 4z^2\}^{\frac{1}{2}}}{r^2}\right] - \frac{1}{\sqrt{2}}[r^2 - 1 + 2z^2 \mp \{(r^2-1)^2 - 4z^2\}^{\frac{1}{2}}]^{\frac{1}{2}}. \tag{19}$$

Since R, r, r_1 are positive, (14) and (16) imply that $0 < \theta_1 < \frac{1}{2}\pi$. Furthermore, we must have $r \geqslant 1$ for z^2 in (18) to be non-negative, and $4z^2 \leqslant (r^2-1)^2$ for $\cos 2\theta_1$ to be real. A check then shows that if (r, z) lies in the region bounded by $z = \pm\frac{1}{2}(r^2 - 1)$, where $r > 1$, there are two values of θ_1, and hence θ, on the circle of latitude determined by the particular (r, z); outside that region there are none (see figure 4). Hence SS lies entirely within the volume of revolution specified in figure 4.

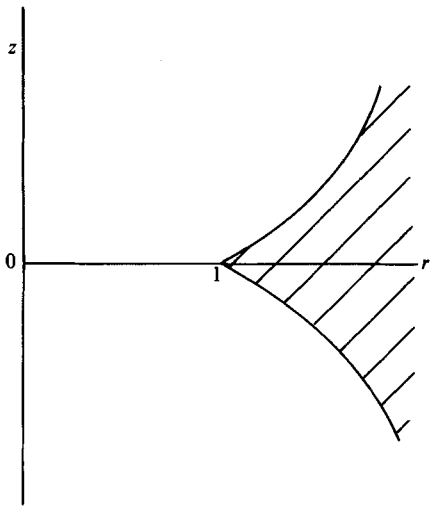

FIGURE 4. The shaded region is bounded by $z = \pm\frac{1}{2}(r^2-1)$. If the diagram is rotated about the polar axis, each point gives rise to a circle; those circles from inside the shaded region intersect SS twice, and those from outside miss it completely.

The Hessian of (13) at stationary points is

$$H = \frac{1}{R^2}\begin{vmatrix} -1 & -r\sin\theta_1 \\ -r\sin\theta_1 & 1-rr_1\cos\theta_1 \end{vmatrix} = \frac{\pm\{(r^2-1)^2-4z^2\}^{\frac{1}{2}}}{R^2}. \tag{20}$$

Since the top left-hand entry in the determinant is negative, it follows that positive H gives a maximum on DS, negative H a saddle. Now on the circles referred to earlier, the two points of intersection with SS correspond to the two signs before the square root; therefore it always happens that one gives a maximum and one a saddle on DS. Thus for a sharp edge, one shock and one logarithmic singularity are situated on each circle of latitude through the shaded part of figure 4, and for a blunt edge two inverse square root singularities occur.

4.2. *Shape of the dividing surface*

We need to sketch the surface $\theta = \theta_1 - R$ at fixed r, z, and determine how its shape depends on r, z. When θ_1 increases by 2π, so does θ; moreover $\theta - \theta_1$ is nearly constant when r_1 is small. Therefore above a neighbourhood of the origin, DS is helicoidal. Exactly above the origin the surface consists of a vertical line, which in the diagrammatic form of figure 2 is a circle through the centre of the solid torus.

The line $\partial\theta/\partial\theta_1 = 0$ has equation $R = rr_1\sin\theta_1$. When $r > 1$ it is a U-shaped curve, shown dashed in figure 5, the minimum and leftmost points being

$$\left.\begin{aligned} \cos\theta_1 &= \frac{1}{r}\left(\frac{r^2-1}{r^2-1+z^2}\right)^{\frac{1}{2}}, & r_1 &= \left(\frac{r^2-1+z^2}{r^2-1}\right)^{\frac{1}{2}}, \\ \cos\theta_1 &= \frac{1}{r}\left\{\frac{(r^2-1)(r^2+z^2)}{r^2-1+z^2}\right\}^{\frac{1}{2}}, & r_1 &= \left\{\frac{(r^2+z^2)(r^2-1+z^2)}{r^2-1}\right\}^{\frac{1}{2}}. \end{aligned}\right\} \tag{21}$$

Inside the U-curve, $\partial\theta/\partial\theta_1 < 0$, and outside, $\partial\theta/\partial\theta_1 > 0$. As $r \to 1$, the whole curve moves up to infinity; when $r < 1$ the U-curve is no longer present, and $\partial\theta/\partial\theta_1 \geqslant 0$

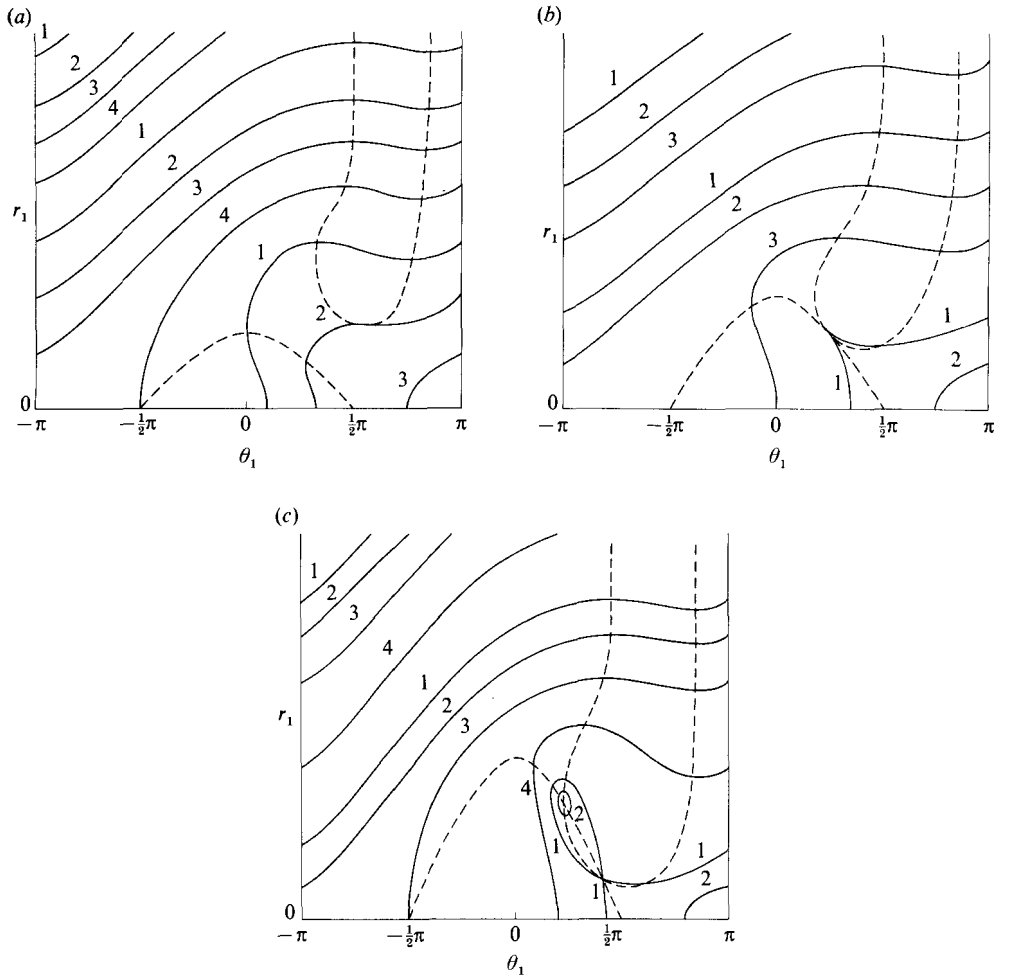

FIGURE 5. Contours of DS in three cases determined by the number of intersections of the dashed lines. Since θ_1 is an angle, contours must be continued over $\theta_1 = \pi$ to coincide with those on the (same) line $\theta_1 = -\pi$, as indicated by the numbering 1, 2, ... In (*b*), contour 1 has a cusp. Note that the disconnected contours labelled 2 in (*c*) have the same value of θ.

everywhere. A similar analysis applies to the line on which $\partial\theta/\partial r_1 = 0$, namely $r_1 = r\cos\theta_1$, also shown dashed. When $r_1 \to \infty$, we have $\theta \to -\infty$.

Critical points on DS occur at the intersections of the two curves just obtained, and figure 5 illustrates the three possibilities. The remarks after (19) give the conditions, in terms of r, z, for the various cases; we also know that when there are two critical points the smaller θ_1 gives a maximum of θ, the larger a saddle. Contours cross the U-curve horizontally and the other dashed curve vertically; in each region the sign of $\mathrm{d}r/\mathrm{d}\theta_1$ is known. The contours are vertical when $r_1 = 0$. For completeness we note that the transitional case of figure 5(*b*) has $|z| = \frac{1}{2}(r^2-1)$ and a critical point

$$\cos\theta_1 = \left(\frac{r^2+1}{2r^2}\right)^{\frac{1}{2}}, \quad r_1 = \left(\frac{r^2+1}{2}\right)^{\frac{1}{2}}. \tag{22}$$

It is also of interest to use coordinates $(x_1, y_1) \equiv (r_1\cos\theta_1, r_1\sin\theta_1)$: the vertical

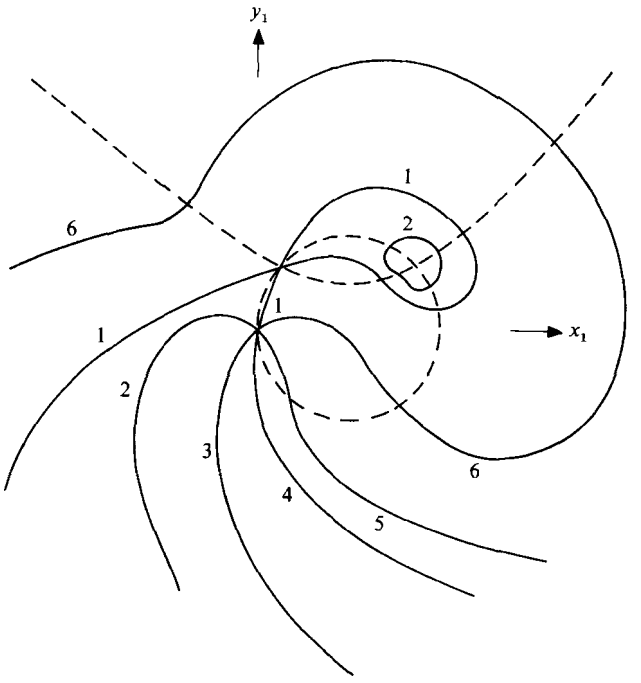

FIGURE 6. Transformation of figure 5(*c*) to the (x_1, y_1)-plane. The contours labelled 2 have the same height; i.e. the retarded propeller edge is disconnected at the corresponding value of θ.

contours on the line $r_1 = 0$ become spokes radiating from a hub at $(x_1, y_1) = (0, 0)$; the lines $\partial\theta/\partial\theta_1 = 0$ and $\partial\theta/\partial r_1 = 0$ become the circle and hyperbola

$$(x_1 - \tfrac{1}{2}r)^2 + y_1^2 = (\tfrac{1}{2}r)^2, \tag{23}$$

$$(r^2 - 1)\, y_1^2 - (x_1 - r)^2 = r^2 + z^2 \quad (y_1 > 0). \tag{24}$$

Figure 6 shows the result when there are two critical points; the other cases are less interesting as each contour simply spirals away from the origin to infinity.

4.3. *The cusped cone*

The shape of SS, defined by (19), will now be built up from sections at constant r, θ, z, using parametric representations in θ_1 obtained from (16)–(18).

4.3.1. *Constant z*

The parameterization when $z \neq 0$ is

$$(r, \theta) = \left(\left\{ \frac{1 + (1 + 4z^2 \cot^2\theta_1)^{\frac{1}{2}}}{2\cos^2\theta_1} \right\}^{\frac{1}{2}}, \quad \theta_1 - \frac{1 + (1 + 4z^2 \cot^2\theta_1)^{\frac{1}{2}}}{2\cot\theta_1} \right), \tag{25}$$

where $0 < \theta_1 < \frac{1}{2}\pi$. Differentiation of r and θ with respect to θ_1 reveals a common factor, vanishing when $\theta_1 = \frac{1}{2}\cos^{-1}\{1/(1 + 2|z|)\}$, where a cusp occurs (see figure 7). The section $z = 0$ has branches $\theta = 0$ and $\theta = \cos^{-1}(1/r) - (r^2 - 1)^{\frac{1}{2}}$, both defined for $r \geqslant 1$.

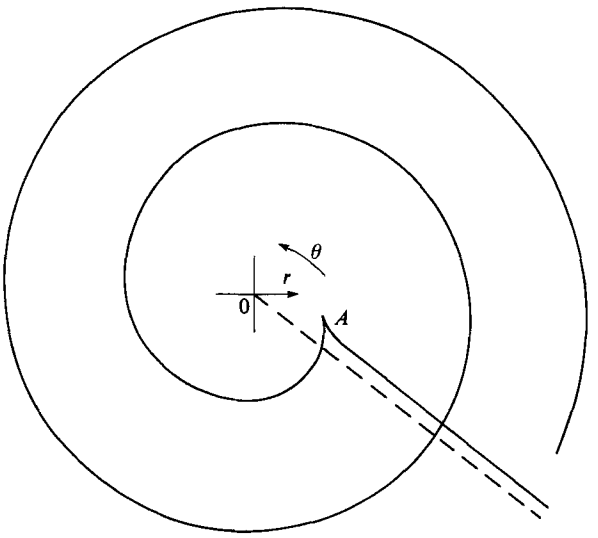

FIGURE 7. Section of SS at positive z. The asymptote $\theta = -z$ is shown. At the cusp, $(r, \theta) = (\{1+2z\}^{\frac{1}{2}}, \frac{1}{2}\cos^{-1}\{1/(1+2z)\} - \{z(1+z)\}^{\frac{1}{2}})$; the slope there is $\mathrm{d}r/\mathrm{d}\theta = -\{(1+z)(1+2z)/z\}^{\frac{1}{2}}$. Asymptotically, $\theta \sim \frac{1}{2}\pi - r$ on the spiral when $r \gg 1$.

4.3.2. *Constant r*

A cylinder of fixed $r > 1$ produces the section

$$(\theta, |z|) = (\theta_1 - \tfrac{1}{2}r^2 \sin 2\theta_1, \quad \tfrac{1}{2}\{(r^2-1)^2 - (r^2\cos 2\theta_1 - 1)^2\}^{\frac{1}{2}}), \tag{26}$$

where $0 < \theta_1 < \frac{1}{2}\cos^{-1}\{(2-r^2)/r^2\}$; the cusp is found at $\theta_1 = \frac{1}{2}\cos^{-1}(1/r^2)$. For large r, the 'arrow-head' (figure 8) may be wrapped several times round the cylinder; note that the semi-angle at the front of the section equals the Mach angle, as would be expected from a local two-dimensional approximation to the propeller's motion.

4.3.3. *Constant θ*

A meridional section at constant θ gives

$$(r, |z|) = \left(\left\{\frac{2(\theta_1 - \theta)}{\sin 2\theta_1}\right\}^{\frac{1}{2}}, \quad \{(\theta_1 - \theta)(\theta_1 - \theta - \tan\theta_1)\}^{\frac{1}{2}}\right), \tag{27}$$

where we must take $\theta < 0$ and θ_1 between 0 and the root of $-\theta = \tan\theta_1 - \theta_1$ in the interval $(0, \frac{1}{2}\pi)$. Cusps occur when $-\theta = \frac{1}{2}\tan 2\theta_1 - \theta_1$ (see figure 9).

4.3.4. *Complete surface*

The size of the arrow-head in figure 8 increases monotonically from zero as r increases from 1 to ∞; in the process, O traces out the propeller edge, B a spiral, together forming the section $z = 0$. Thus the whole surface is a cusped cone, comprising three smooth sheets sewn together tangentially along the cusped edges and non-tangentially along the third edge. Near the vertex, parametric equations for the surface and cusp lines are

$$(r, \theta, z) \approx (1+\epsilon, -2\theta_1(\epsilon - \tfrac{1}{3}\theta_1^2), \pm\theta_1(2\epsilon - \theta_1^2)^{\frac{1}{2}}) \tag{28}$$

$$= (1+\epsilon, -\tfrac{4}{3}\epsilon^{\frac{3}{2}}, \pm\epsilon), \tag{29}$$

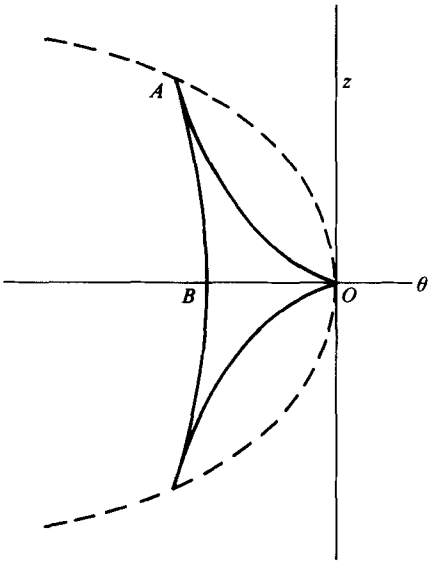

FIGURE 8. Section of SS by a cylinder of radius $r > 1$. The upper cusp has coordinates $(\theta, z) = (\frac{1}{2}\{\cos^{-1}(1/r^2) - (r^4-1)^{\frac{1}{2}}\}, \frac{1}{2}\{r^2-1\})$, and the slope of SS there is $\mathrm{d}z/\mathrm{d}\theta = -\{(r^2+1)/(r-1)\}^{\frac{1}{2}}$. Point B, where $z = 0$, has parameter $\theta_1 = \frac{1}{2}\cos^{-1}\{(2-r^2)/r^2\}$ and position $\theta = \frac{1}{2}\cos^{-1}\{(2-r^2)/r^2\} - (r^2-1)^{\frac{1}{2}}$. At the origin, $\mathrm{d}z/\mathrm{d}\theta = \pm r/(r^2-1)^{\frac{1}{2}}$. As r varies, the cusps trace out the dashed curve; its equation is $|z| \sim (-\frac{3}{4}\theta)^{\frac{2}{3}}$ when $r \approx 1$ and $|z| \sim -\theta + \frac{1}{4}\pi - \frac{1}{2}$ when $r \gg 1$.

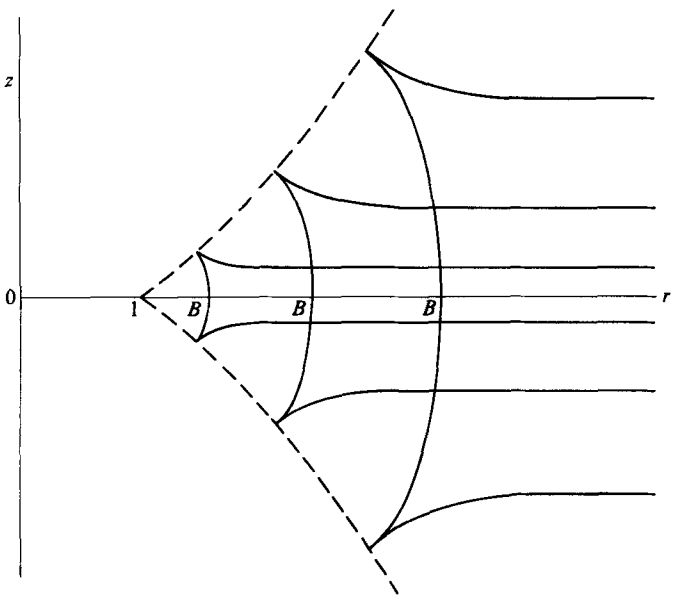

FIGURE 9. Section of SS by a meridional plane θ; note that $-2\pi < \theta < 0$ and we have superposed $\theta - 2n\pi$ for $n = 1, 2, \ldots$. Asymptotically, $|z| \sim -(\theta - 2n\pi)$ for $r \gg 1$. The upper cusps lie on $z = \frac{1}{2}(r^2-1)$ and have coordinates $(r, z) = (\{\sec 2\theta_1\}^{\frac{1}{2}}, \frac{1}{2}\{\sec 2\theta_1 - 1\})$, where the values of θ_1 satisfy $-\theta = \frac{1}{2}\tan 2\theta_1 - \theta_1$; the slope of SS at a cusp is $\mathrm{d}z/\mathrm{d}r = -\sqrt{2}\sin\theta_1$. Points B, for which $z = 0$, are given by $r = \sec\theta_1$, with $-\theta = \tan\theta_1 - \theta_1$.

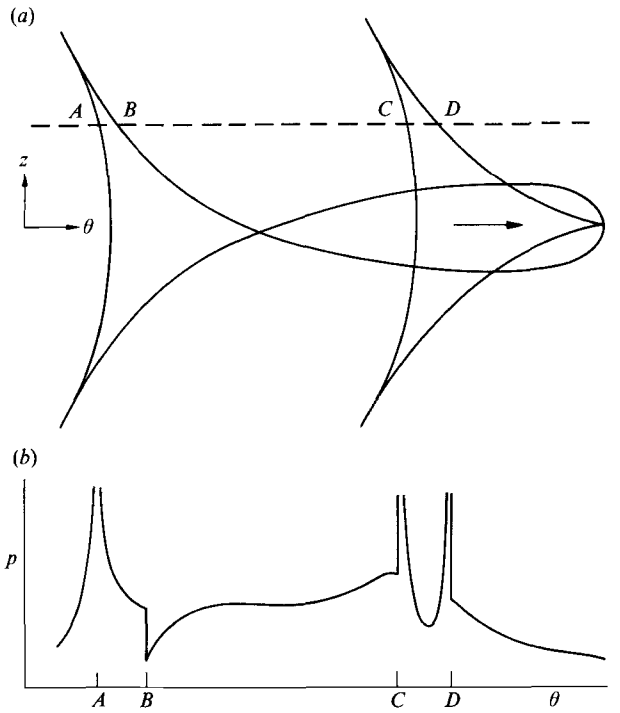

FIGURE 10. (*a*) Section at fixed r of a blade with blunt leading edge and sharp trailing edge, showing sections of the cones. (*b*) Schematic graph of pressure as a function of θ along the dashed line in (*a*), indicating A: logarithmic spike; B: finite jump; C, D: inverse square root.

respectively, where in the former $0 \leqslant \theta_1 \leqslant (2\epsilon)^{\frac{1}{2}} \ll 1$, and in the latter $\epsilon = \theta_1^2$. The cone is flattened almost to a plane in this region, since $r-1$ and z are $O(\epsilon)$, whereas θ is $O(\epsilon^{\frac{3}{2}})$.

4.4. *Shocks and singularities on the cone*

Although H and R in §3.2 are usually complicated functions of position, they simplify for a radial edge, because (20) gives $(R(\pm H)^{\frac{1}{2}})_c = \Gamma$, where

$$\Gamma = \left[\left\{\left(\frac{r\Omega}{c}\right)^2 - 1\right\}^2 - 4\left(\frac{z\Omega}{c}\right)^2\right]^{\frac{1}{4}}; \tag{30}$$

we have reverted to dimensional variables, so that r and z are lengths. Now the cusp lines lie in the surface $\Gamma = 0$; hence on the cone, the strength of shock or singularity tends to infinity as a cusp is approached, in proportion to the inverse quarter power of distance from the cusp line. Such behaviour is well-known from Tricomi's equation (Gill & Seebass 1975).

The sign of the determinant in (20) may be found using the formulae of §4.3; these reveal that on the front sheets of the cone, i.e. between the propeller edge and the cusp lines, there corresponds a maximum of DS, while on the rear sheet, i.e. between the two cusp lines, there corresponds a saddle. Hence a sharp edge produces a shock on the front of the cone and a logarithmic singularity on the rear, whereas a blunt edge produces inverse square root singularities on both; in the latter case, the sides on which the pressure is infinite are different for the front and rear, by §§3.2.3 and 3.2.4.

These results can be illustrated and summarized by considering a propeller with a blunt leading edge and sharp trailing edge. Figure 10(*a*) superimposes the sections of the blade and cones at fixed r; the dashed line intersects the cones at $\theta = \theta_A, \ldots, \theta_D$ to give the typical graph of p against θ shown in figure 10(*b*). Then near A, B, C, D we obtain from §3.2 the following expressions for the discontinuous or singular component:

$$p_{\mathrm{S}}^{(A)} = \frac{\rho_0 \Omega^2}{\pi} \frac{(r_1 g^+)_{\mathrm{c}}}{\Gamma} \ln\left(\frac{1}{|\theta - \theta_A|}\right), \tag{31}$$

$$\Delta p^{(B)} = -\rho_0 \Omega^2 \frac{(r_1 g^+)_{\mathrm{c}}}{\Gamma}, \tag{32}$$

$$p_{\mathrm{S}}^{(C)} = -\rho_0 \Omega^2 \frac{(r_1 g_1^-)_{\mathrm{c}}}{\Gamma} \frac{1}{(\theta - \theta_C)^{\frac{1}{2}}} \quad (\theta > \theta_C), \tag{33}$$

$$p_{\mathrm{S}}^{(D)} = -\rho_0 \Omega^2 \frac{(r_1 g_1^-)_{\mathrm{c}}}{\Gamma} \frac{1}{(\theta_D - \theta)^{\frac{1}{2}}} \quad (\theta < \theta_D). \tag{34}$$

5. Discussion

By the method of §3, formulae as detailed as those of §4 may be obtained for any edge of known equation $h(r, \theta) = 0$; a straightforward extension includes the effect of blade tips. For a propeller with axial velocity as well as rotation, the generalization of (1)–(4) given in Hanson (1976) may likewise be analysed. But only thickness noise yields to the method, since the linear loading problem gives an integral equation, not an explicit solution of the form (4).

The results obtained above may be interpreted in terms of rays: rotation of the cusped cone with the propeller is identical to propagation of the cone surface normal to itself at the speed of sound, and the cusp line is caused by focusing of the front sheets of the cone, on their way to becoming the rear sheets. Thus the nonlinear problem which must be solved to eliminate the singularities is equivalent to that of the focusing of a weak shock. This requires a transonic equation (Guiraud 1965); the weakly nonlinear theory of Whitham (1956) is not sufficient, because it too would predict a singularity at the cusp line, thereby violating the assumption on which that theory is based. Even when only the far field is required, any focusing on the linear theory makes nonlinear analysis difficult, because some of the rays pass through the transonic focusing region on the way out; the analysis presented in Tam & Salikuddin (1986) would therefore seem to be restricted to directions in which focusing does not occur. These remarks are in agreement with Caradonna & Isom (1972) and Hawkings (1979), who discuss the necessity for transonic equations at tip speeds in the supersonic or high subsonic range. It should be noted that the lines of focusing on linear theory may spiral out to infinity even if only a small section of an edge is supersonic.

Since the equations of transonic flow are so different from those of acoustics, one might ask whether the linear results of this paper are helpful even as a first step towards the nonlinear theory. The experimental results of Sturtevant & Kulkarny (1976) on the focusing of weak shock waves are relevant here; their photographs clearly show that for weak enough shocks the cusped surface of linear theory is present, but the pressure has a finite hump in place of a singularity. Thus one would expect some trace of the cusped cone in the exact nonlinear solution of the propeller problem, if the blades are thin enough.

The author would like to thank C. L. Morfey for his suggestion of supersonic propeller acoustics as a promising area of research, and for his encouragement throughout the course of the work. Thanks are also due to M. J. Fisher and G. M. Lilley for many interesting and informative discussions. The work was carried out at the Institute of Sound and Vibration Research in the University of Southampton, and was funded by the Ministry of Defence through the Royal Aircraft Establishment; an early version of the paper benefited from a visit of the author to NASA Lewis Research Center as a Case/NASA Research Fellow.

Appendix. Evaluation of integrals

On changing the notation to a conventional form, we require

$$I(z) = \int_{-\infty}^{\infty} \int_{-\infty}^{\infty} f(x, y, z)\, \mathrm{d}x\, \mathrm{d}y, \tag{A 1}$$

where f is discontinuous or singular on a surface DS: $z = s(x, y)$. The origin is assumed to be a stationary point of DS, so that $s = s_x = s_y = 0$ at $(x, y) = (0, 0)$, and $z = 0$ is a critical value; hence near the origin, DS and its Hessian are

$$z = s(x, y) \approx ax^2 + 2hxy + by^2 \tag{A 2}$$

and

$$H = 4(ab - h^2), \tag{A 3}$$

where a, b, h are constants. Two cases only will be examined: first, $a > 0$, $b > 0$, $ab > h^2$, which gives DS a local minimum at the origin; and second, $ab < h^2$, which gives DS a saddle point. The results for a local maximum of DS follow by transformation. We shall not deal with examples such as $ab = h^2$ or a, b, h all zero, though their analysis is not difficult.

The only relevant aspect of $I(z)$ is its non-smooth part near $z = 0$ due to the different behaviour of f on the two sides of DS. By subtraction of a function smooth everywhere, f may be taken to be zero when $z < s(x, y)$. Suitable forms when $z > s(x, y)$ are

$$f(x, y, z) = \begin{cases} f_0 + px + qy + rz + \ldots & \text{(sharp)}, \\ \dfrac{f_0 + px + qy + rz + \ldots}{\{z - s(x, y)\}^{\frac{1}{2}}} & \text{(blunt)}, \end{cases} \tag{A 4}$$

for the two types of trailing edge; leading edges require a simple transformation to make f zero above DS. The various cases will now be treated in turn; §A.1 and §A.2 below are covered by Friedlander (1958). A subscript s on I will denote the singular part.

A.1. *Sharp edge; extremum*

The surface DS is approximated by (A 2) with positive a, b, $ab - h^2$; hence a plane of constant positive z intersects the region above DS in an ellipse enclosing area $\pi z/(ab - h^2)^{\frac{1}{2}}$, whereas if $z < 0$ the plane lies entirely below DS. Thus

$$I'(z) \approx \begin{cases} \dfrac{2\pi f_0}{H^{\frac{1}{2}}} & (z > 0), \\ 0 & (z < 0). \end{cases} \tag{A 5}$$

Further analysis gives an error term in (A 5), due to terms beyond f_0 in f and beyond quadratic in (A 2), of size $O(z)$; therefore the jump in I' at $z = 0$ is exactly $2\pi f_0/H^{\frac{1}{2}}$.

A.2. *Sharp edge*; *saddle*

If DS is approximated by (A 2) with $ab < h^2$, a plane of constant z intersects the region above DS in an area bounded by two branches of a hyperbola; as shown in figure 3(*b*), the area may be connected or in two parts, transition occurring at $z = 0$. Now in the special case $s(x, y) = xy$, the area of the region $xy < z$, $|x| < 1$, $|y| < 1$ when $|z| < 1$ is $2(1+z-z\ln|z|)$. Since the Hessian acts merely as a scaling factor, the dominant part of I' is

$$I'_s(z) = \frac{2f_0}{(-H)^{\frac{1}{2}}} \ln\left(\frac{1}{|z|}\right) + O(z\ln|z|). \tag{A 6}$$

A.3. *Blunt edge*; *extremum*

The special case $s(x, y) = x^2+y^2$ requires the integral of $(z-x^2-y^2)^{-\frac{1}{2}}$ over the disk $x^2+y^2 < z$, when $z > 0$; this gives $2\pi z^{\frac{1}{2}}$. Scaling by the Hessian leads to

$$I'_s(z) = \frac{2\pi f_0}{H^{\frac{1}{2}}} \frac{1}{z^{\frac{1}{2}}} + O(z^{\frac{1}{2}}) \quad (z > 0). \tag{A 7}$$

A.4. *Blunt edge*; *saddle*

Integration of $(z-xy)^{-\frac{1}{2}}$ over the region specified in §A.2 produces a rather complicated analytic function, plus, for $z < 0$, a term $-4\pi(-z)^{\frac{1}{2}}$. Scaling leads to

$$I'_s(z) = \frac{2\pi f_0}{(-H)^{\frac{1}{2}}} \frac{1}{(-z)^{\frac{1}{2}}} + O((-z)^{\frac{1}{2}}) \quad (z < 0). \tag{A 8}$$

REFERENCES

Blackburn, H. W. 1984 Sound sources on high-speed surfaces. PhD thesis, University of Cambridge.

Caradonna, F. X. & Isom, M. P. 1972 Subsonic and transonic potential flow over helicopter rotor blades. *AIAA J.* **10**, 1606–1612.

Cramer, M. S. & Seebass, A. R. 1978 Focusing of weak shock waves at an arête. *J. Fluid Mech.* **88**, 209–222.

Farassat, F. 1975 Theory of noise generation from moving bodies with an application to helicopter rotors. *NASA TR* R-451.

Friedlander, F. G. 1958 *Sound Pulses.* Cambridge University Press.

Gill, P. M. & Seebass, A. R. 1975 Nonlinear acoustic behaviour at a caustic: an approximate analytical solution. *Prog. Astronaut. Aeronaut.* **38**, 353–386.

Guiraud, J.-P. 1965 Acoustique géométrique, bruit balistique des avions supersoniques et focalisation. *J. Méc.* **4**, 215–267.

Hanson, D. B. 1976 Near field noise of high tip speed propellers in forward flight. *AIAA paper* 76-565, presented at 3rd AIAA aeroacoustics conference, Palo Alto.

Hawkings, D. 1979 Noise generation by transonic open rotors. *Res. Paper* 599, Westland Helicopters Ltd, Yeovil, England.

Hawkings, D. L. & Lowson, M. V. 1974 Theory of open supersonic rotor noise. *J. Sound Vib.* **36**, 1–20.

Hayes, W. D. 1971 Sonic Boom. *Ann. Rev. Fluid Mech.* **3**, 269–290.

Lilley, G. M., Westley, R., Yates, A. H. & Busing, J. R. 1953 Some aspects of noise from supersonic aircraft. *J. R. Aero. Soc.* **57**, 396–414.

Lowson, M. V. & Jupe, R. J. 1974 Wave forms for a supersonic rotor. *J. Sound Vib.* **37**, 475–489.

Obermeier, F. 1983 On the propagation of weak and moderately strong, curved shock waves. *J. Fluid Mech.* **129**, 123–136.

Rao, P. S. 1956 Supersonic bangs, parts I and II. *Aero. Q.* **7**, 21–44 and 135–155.

SCHWARTZ, I. R. (ed.) 1968 Second conference on sonic boom research. *NASA SP*-180.

SCHWARTZ, I. R. (ed.) 1971 Third conference on sonic boom research. *NASA SP*-255.

SEEBASS, A. R. (ed.) 1967 Sonic boom research. *NASA SP*-147.

STURTEVANT, B. & KULKARNY, V. A. 1976 The focusing of weak shock waves. *J. Fluid Mech.* **73**, 651–671.

TAM, C. K. W. 1983 On linear acoustic solutions of high speed helicopter impulsive noise problems. *J. Sound Vib.* **89**, 119–134.

TAM, C. K. W. & SALIKUDDIN, M. 1986 Weakly nonlinear acoustic and shock-wave theory of the noise of advanced high-speed turbopropellers. *J. Fluid Mech.* **164**, 127–154.

WANNER, J.-C. L., VALLEE, J., VIVIER, C. & THERY, C. 1972 Theoretical and experimental studies of the focus of sonic booms. *J. Acoust. Soc. Am.* **52**, 13–32.

WARREN, C. H. E. 1968 Sonic bangs. In *Noise and Acoustic Fatigue in Aeronautics* (ed. E. J. Richards & D. J. Mead), pp. 266–284. Wiley.

WHITHAM, G. B. 1956 On the propagation of weak shock waves. *J. Fluid Mech.* **1**, 290–318.